

# Implications for the origin of short gamma-ray bursts from their observed positions around their host galaxies

Ross P. Church<sup>1\*</sup>, Andrew J. Levan<sup>2,1</sup>, Melvyn B. Davies<sup>1</sup> and Nial Tanvir<sup>3</sup>

<sup>1</sup>*Lund Observatory, Box 43, SE-221 00, Lund, Sweden.*

<sup>2</sup>*Department of Physics, University of Warwick, Coventry, CV4 7AL*

<sup>3</sup>*Department of Physics and Astronomy, University of Leicester, Leicester, LE1 7RH, UK.*

Accepted 2011 January 4. Received 2010 November 17; in original form 2010 January 7.

## ABSTRACT

We present the observed offsets of short-duration gamma-ray bursts (SGRBs) from their putative host galaxies and compare them to the expected distributions of merging compact object binaries, given the observed properties of the hosts. We find that for all but one burst in our sample the offsets are consistent with this model. For the case of bursts with massive elliptical host galaxies, the circular velocities of the hosts' haloes exceed the natal velocities of almost all our compact object binaries. Hence the extents of the predicted offset distributions for elliptical galaxies are determined largely by their spatial extents. In contrast, for spiral hosts the galactic rotation velocities are smaller than typical binary natal velocities and the predicted burst offset distributions are more extended than the galaxies.

One SGRB, 060502B, apparently has a large radial offset that is inconsistent with an origin in a merging galactic compact binary. Although it is plausible that the host of GRB 060502B is mis-identified, our results show that the large offset is compatible with a scenario where at least a few per cent of SGRBs are created by the merger of compact binaries that form dynamically in globular clusters.

**Key words:** Gamma-ray bursts: compact binaries: supernovae

## 1 INTRODUCTION

The merger of a compact binary consisting of neutron stars (NSs) or black holes (BHs) is a prime model for the origin of the short-duration gamma-ray bursts (SGRBs). Compact binaries may be formed by numerous channels including those which are formed in primordial binaries (Belczynski et al. 2002), and those which are formed dynamically in dense cluster cores (e.g. Davies 1995; Grindlay et al. 2006). Once formed the binary loses energy and angular momentum from its orbit in the form of gravitational radiation, and the compact objects spiral together and eventually merge. The merger time is highly sensitive to both separation and eccentricity and thus has an extremely broad distribution.

Evidence for the origin of SGRBs in the final coalescence of such systems potentially comes both from the host galaxy types (e.g. Zheng & Ramirez-Ruiz 2007) and the measured offsets of SGRBs from their hosts (e.g. Bloom et al. 1999; Belczynski et al. 2006; Troja et al. 2008). The kicks imparted to double compact object (DCO) systems on formation, both in terms of dynamical kicks to the

binary and natal kicks to neutron stars, endow DCO binaries with spatial velocities of up to several hundred  $\text{km s}^{-1}$ . This means that they may merge far from their birth sites, even outside their parent galaxies. Equally, if the inspiral takes  $> 10^8$  years, then the host galaxy may no longer exhibit significant ongoing star formation at the time of merger.

Observations of SGRBs obtained by *Swift* so far offer broad support for this picture. Several of the host galaxies observed are old (Gehrels et al. 2005; Berger et al. 2005; Barthelmy et al. 2005; Bloom et al. 2006), while only a small fraction are starbursts. However, the sample has been building up slowly, and we are only now approaching a stage where it is possible to compare the observed offsets with predictions for DCO binaries. We build on previous work that modelled the offset distributions of DCO mergers (e.g. Bloom et al. 1999; Fryer et al. 1999) by using the observed properties of the host galaxies to predict offset distributions on a host-by-host basis.

In this paper we take the observed sample of SGRBs that have identified hosts and model the production and galactic trajectories of DCO binaries inside those hosts. In Section 2 we review the sample of bursts; we describe our models in Section 3, discussing the results and possible se-

\* email: ross@astro.lu.se

GRB	Satellite	$t_{90}$ s	Opt	Host Mag.	Host $M_B$	$z$	Type	$R_e$ kpc	$R_{\text{proj}}$ kpc	$R_{\text{err}}$ kpc	References
050509B	<i>Swift</i>	0.04	No	$16.75 \pm 0.05$	-23.25	0.225	E	20.98	63.7	12.1	(a), (b)
050709	<i>HETE-2</i>	0.07	Yes	$21.05 \pm 0.07$	-18.19	0.161	S/I	1.75	3.55	0.27	(c), (d), (b)
050724	<i>Swift</i>	3.0	Yes	$18.19 \pm 0.03$	-22.11	0.257	E	4.00	2.54	0.08	(e), (b)
051221A	<i>Swift</i>	1.4	Yes	$21.81 \pm 0.09$	-20.20	0.546	S	2.17	1.53	0.31	(f), (g)
060502B	<i>Swift</i>	0.05	No	$18.71 \pm 0.01$	-21.84	0.287	E	10.5	73	13	(h)
060801	<i>Swift</i>	0.5	No	$22.97 \pm 0.11$	-20.64	1.130	S	-	19.7	14.0	(i), (j)
061006	<i>Swift</i>	0.4	Yes	$22.65 \pm 0.09$	-18.86	0.438	S	3.67	1.44	0.29	(b)
061201	<i>Swift</i>	0.8	Yes	$19.65 \pm 0.10$	-18.76	0.111	S	1.8	33.9	0.4	(i), (j)
061210	<i>Swift</i>	0.2	No	$21.00 \pm 0.02$	-20.36	0.410	S	-	10.7	6.9	(i), (j)
061217	<i>Swift</i>	0.3	No	$23.33 \pm 0.07$	-19.61	0.827	S	-	55	20	(i), (j)
070429B	<i>Swift</i>	0.5	Yes	$23.22 \pm 0.10$	-19.91	0.902	S	-	4.7	4.7	(k)
070714B	<i>Swift</i>	2.0	Yes	$24.92 \pm 0.23$	-18.26	0.923	S	-	3.08	0.47	(l)
070724A	<i>Swift</i>	0.4	Yes	$20.53 \pm 0.03$	-21.07	0.457	E	-	4.76	0.06	(m)
070809	<i>Swift</i>	1.3	Yes	$21.7 \pm 0.3$	-18.23	0.219	S	-	19.61	1.9	(n)
071227	<i>Swift</i>	1.8	Yes	$20.54 \pm 0.03$	-20.73	0.394	S	-	16.1	0.2	(o)
080905A	<i>Swift</i>	1.0	Yes	$18.0 \pm 0.5$	-20.63	0.122	S	-	18.11	0.42	(p)

**Table 1.** Properties of SGRBs with known X-ray, optical or radio counterparts. Data is taken from the literature sources indicated other than for a small number of the offsets which we have re-measured in described in Section 2. Columns list in order: the burst identifier, the satellite which detected the burst, the duration over which 90% of the total fluence was seen ( $t_{90}$ ), whether an optical counterpart was detected, the host apparent  $R$ -band magnitude and error, the host absolute  $B$ -band magnitude, the redshift, the host type (spiral/elliptical), the host effective radius  $R_e$ , the offset  $R_{\text{proj}}$  and the error on the offset  $R_{\text{err}}$ . The duration,  $t_{90}$ , is measured in the 15-350 keV range for the *Swift* bursts and in the 30-400 keV range for the *HETE-2* burst. The absolute magnitudes have been calculated assuming a source with a flat spectrum in  $F_\nu$ . All offset errors are one-sigma; 90% confidence limits in the literature have been converted assuming a Gaussian PSF. References: (a) Gehrels et al. (2005); (b) Fong et al. (2009); (c) Fox et al. (2005); (d) Villasenor et al. (2005); (e) Berger et al. (2005); (f) Soderberg et al. (2006); (g) this work; (h) Bloom et al. (2007); (i) Berger et al. (2007); (j) Troja et al. (2008); (k) Cenko et al. (2008); (l) Graham et al. (2009); (m) Berger et al. (2009); (n) Perley et al. (GCN 7889); (o) D’Avanzo et al. (2009); (p) Rowlinson et al. in prep.

lection effects in Section 4. The alternative possibility of DCO binaries forming dynamically in the cores of globular clusters is discussed in Section 5.

## 2 THE BURSTS AND THEIR HOST GALAXIES

From the set of observed short GRBs we have selected the bursts with positions localised through observations of their X-ray and, where possible, optical afterglows. Furthermore we have discarded bursts without identified host galaxies or for which there are not robust redshift measurements, since knowledge of the redshift is necessary to construct model galactic potentials. For several bursts we have re-analysed available data to perform relative astrometry at times when the afterglow was bright, mapping the locations of the burst onto the hosts utilising the `geomap` task within IRAF and a number of point sources within the field. For other bursts we have used offsets available in the literature. Our final sample of 16 bursts is listed in Table 1.

In order to obtain dynamical models for the bursts’ host galaxies we split the sample into elliptical and spiral hosts. In both cases we adopt the logarithmic profile of Thomas et al. (2009) to model the host galaxy’s dark halo,

$$\rho = \frac{v_h}{4\pi G} \frac{3r_h^2 + r^2}{(r_h^2 + r^2)^2}, \quad (1)$$

where  $r_h$  is the core radius of the halo and  $v_h$  its circular velocity at infinity. This profile is constructed such that the circular velocity approaches  $v_h$  asymptotically at infinity.

It should be noted that as elliptical galaxies do not have discs in their case the circular velocity is not directly measurable, but it is useful to parameterise the potential in the same way. Initially we place the binaries in an exponential disc, chosen so that half the stars are within the effective radius. For elliptical hosts we use the scaling relations of Thomas et al. (2009) to obtain the properties of the galaxy’s halo from its blue-band magnitude. The effective radius  $R_e$  is taken from Gerhard et al. (2001) as cited by Thomas et al. (2009). The properties of spiral galaxies are taken from Kormendy & Freeman (2004). The complete set of models that we used are given in Table 2. We take  $R_e$  to be the half-light radius of the galaxy. A comparison between the observed and predicted  $R_e$  shows that there is considerable scatter, as would be expected from observations of galaxy properties (see e.g. figure 3 of Thomas et al. 2009). Where a galaxy has an observed  $R_e$  we compute models using both the value predicted by the formula and the measured value, and use the observational value in preference (for example, in the cumulative offset distributions of Figures 8 and 10).

## 3 POPULATION SYNTHESIS AND GALACTIC TRAJECTORIES

To model the observed DCO populations we conduct a population synthesis of NS–NS and BH–NS binaries, utilising the rapid binary population synthesis code BSE (Hurley et al. 2002). We have modified BSE following Belczynski et al. (2002) and Belczynski et al. (2008) to include a more realistic prescription for compact object masses, hypercritical

GRB	Type	$v_h$ km s <sup>-1</sup>	$r_h$ kpc	$R_e$ kpc	$R_e^{\text{obs}}$ kpc	$M_h$ 10 <sup>11</sup> $M_\odot$
050509B	E	663.74	46.34	24.54	20.98	205
050709	S	109.63	7.90	0.91	1.75	0.41
050724	E	532.40	23.92	8.41	4.0	19.4
051221A	S	157.30	15.66	2.42	2.17	0.82
060502B	E	505.31	20.45	6.52	10.5	60.1
060801	S	170.23	18.20	3.00		1.48
061006	S	123.65	9.92	1.26	3.67	1.22
061201	S	121.45	9.59	1.20	1.80	0.48
061210	S	161.88	16.54	2.62		1.14
061217	S	141.48	12.81	1.81		0.56
070429B	S	149.31	14.19	2.10		0.75
070714B	S	111.02	8.90	0.94		0.14
070724A	E	435.39	13.08	3.17		11.9
070809	S	110.42	8.00	0.92		0.15
071227	S	173.00	18.77	3.13		1.60
080905A	S	169.92	18.14	2.98		1.46

**Table 2.** Parameters of the galactic models that we used. Columns list the GRB, whether the host is spiral or elliptical, the asymptotic rotational velocity of the halo model  $v_h$ , the halo core radius  $r_h$ , the predicted effective radius  $R_e$  and, where one is available, the observed effective radius  $R_e^{\text{obs}}$ . The final column is the mass enclosed within a spherical radius of  $10 R_e$ , which acts as an indicative halo mass.

accretion during common envelope evolution, and delayed dynamical instability in mass transfer from helium stars in binaries with a large mass ratio. More details of our population synthesis code, and the constraints which can be placed on DCO formation will be presented in a later paper (Church et al. in prep.). For reasons of simplicity we distribute stellar masses according to the Kroupa et al. (1993) IMF, selecting both stars independently from the IMF and only considering stars with masses greater than  $3 M_\odot$ . Binary semi-major axes are chosen from a distribution flat in  $\log a$  between 1 and  $10^4 R_\odot$ . Preliminary simulations showed that binaries wider than this do not contribute to the DCO population. The initial eccentricity of the binaries has little effect on their evolution and is set equal to 0.1 for all binaries.

### 3.1 Neutron star kicks

For the purpose of modelling the galactic offsets of SGRBs the most significant uncertainty is the natal kick imparted to neutron stars at their formation. In this paper we utilise two distributions of neutron star natal kicks: the bimodal kick distribution of Arzoumanian et al. (2002), henceforth ACC02, and the Maxwellian distribution recommended by Dewi et al. (2005), henceforth DPP05.

The ACC02 distribution leads to strong kicks, with typical magnitudes of several hundred km s<sup>-1</sup>, and is derived from observations of isolated pulsars. The DPP05 distribution yields much smaller kicks – the dispersion is only 20 km s<sup>-1</sup> – and is derived from constraints placed on the space velocity of the second neutron star formed in a binary by the relationship between its spin and orbital eccentricity. We also computed models that utilised the distribution of Hansen & Phinney (1997), but this produced results that were, for our purposes, very similar to those obtained with the ACC02 distribution.

We specify the natal kick distributions for the two objects that form in each DCO separately, considering three combinations of kick distributions. In the first scenario both compact objects receive an ACC02 (strong) kick. Alternatively, the first compact object to form may receive an ACC02 (strong) kick and the second a DPP05 (weak) kick. Finally both objects may receive a DPP05 (weak) kick. As the evidence for weak kicks relies on the properties of the second compact object we do not consider the case where the first kick is weak and the second kick is strong.

A powerful test of the neutron star kick distributions is the comparison of the synthesised NS–NS binary populations that they yield with the properties of observed NS–NS binaries. In particular, the kicks very strongly affect the semi-major axis  $a$  and eccentricity  $e$  of a given DCO binary. The ability of a kick distribution to produce the observed NS–NS binaries in the  $a, e$  plane is a stringent test of its correctness. We present the  $a, e$  distribution of all the NS–NS binaries formed in our simulations in Figure 1.

There is little evidence as to whether a kick is imparted to black holes at formation (Belczynski et al. 2008), though for the Galactic black-hole binary Cygnus X–1 there is evidence that there was no substantial natal kick (Mirabel & Rodrigues 2003). A significant kick would require the asymmetric ejection of a large fraction of the progenitor’s envelope, rather than its accretion onto the black hole. The larger mass of a typical black hole compared to a neutron star increases the quantity of mass that must be ejected to produce a significant kick. Hence we choose not to apply a natal kick to black holes upon formation. Where a black hole forms via the accretion-induced collapse of a neutron star we of course apply a kick to that neutron star at its birth. We have tested the effect of omitting black hole kicks by synthesising a population of BH–NS binaries where a kick following the ACC02 distribution is applied, reduced according to the ratio of the typical neutron star mass to the nascent black hole mass. This is equivalent to a natal kick with the same distribution of impulses as a neutron star kick. We found that the space velocity distribution of the binaries that we produced was largely unaffected. This is unsurprising as such binaries are typically rather massive and hence strongly bound at the time of the kick and, as our results show, the properties of our sample of DCO binaries is relatively insensitive to the natal kick chosen for the first supernova.

In addition to the natal kicks each supernova causes an impulse to the binary by the rapid loss of a large quantity of mass. As this mass escapes anisotropically it takes away a significant net momentum. This effect is also taken into account in our simulations and accounts for the fact that, even when two small kicks are utilised, a DCO binary may have a large spatial velocity after formation.

We plot the mass lost in the final supernova as a function of the orbital separation immediately prior to the supernova for all potential DCO progenitors in Figures 2 (NS–NS binaries) and 3 (BH–NS binaries). In each case the upper panel shows binaries that are bound after the supernova and natal kick, whilst the lower panel includes systems that unbind at the final supernova and hence form two isolated compact objects. In both cases the natal kick distribution is that which we prefer for the subsequent analysis, the ACC02 distribution (see Section 4.1). It is apparent in both cases

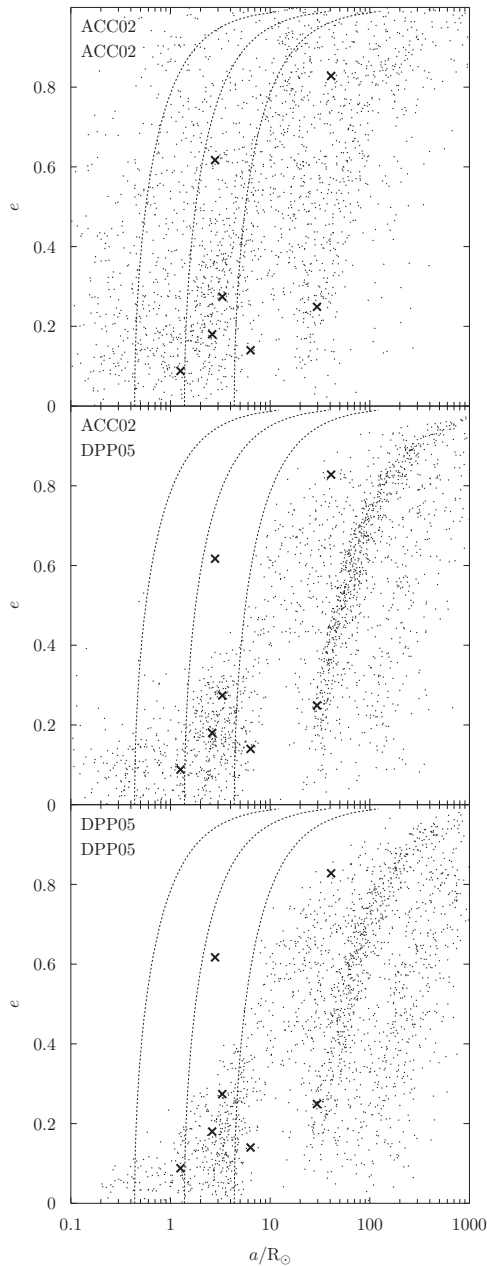


**Figure 1.** Dots show the eccentricity  $e$  as a function of semi-major axis  $a$  for our synthesised populations of NS–NS binaries, plotted in the location in which they form. To clarify the plots only 2000 binaries are plotted in each case. Crosses show the properties of the observed NS–NS binaries. Lines of iso-merger-time of  $10^6$ ,  $10^8$  and  $10^{10}$  yr are also plotted. The three panels show different combinations of kick distributions. Top: ACC02 kick for both NSs. Middle: ACC02 kick for the first NS and DPP05 kick for the second NS. Bottom: DPP05 kick for both NSs.

that the pre-supernova binaries fall into two groups, one with large separations and one with small separations. The large separation group tend to also have larger mass-loss, as they have not gone through a recent episode of common-envelope evolution and hence the progenitor of the second compact object retains a larger fraction of its envelope. These wider binaries are usually disrupted by the final supernova, un-

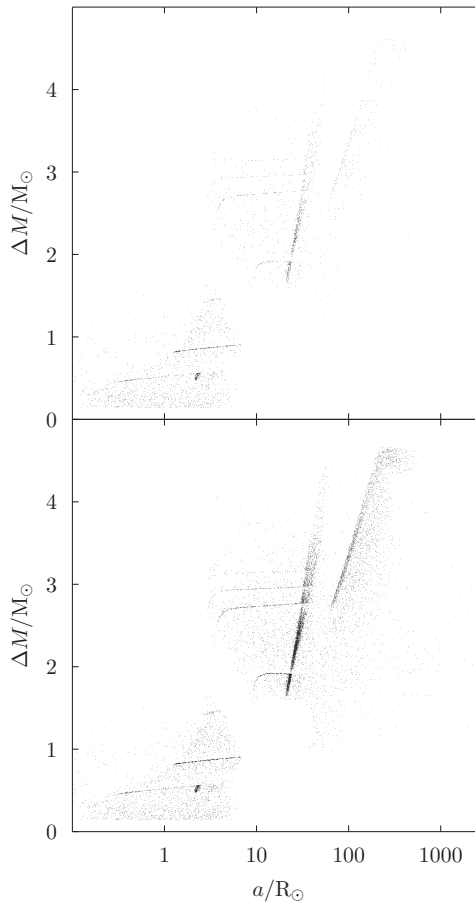


**Figure 2.** Dots show the mass lost in the final supernova,  $\Delta M$ , as a function of pre-supernova semi-major axis  $a$  for the binaries that potentially form a NS–NS binary. The bottom panel shows all binaries that are bound prior to the final supernova, the upper panel only the subset that remain bound subsequent to the final supernova. The ACC02 kick distribution was used for both kicks.

less a chance alignment of natal kick causes them to remain bound. In the case where they do produce a bound binary it is usually wide enough that it does not merge under the effects of gravitational wave radiation within the Hubble time<sup>1</sup> and hence is not significant for our calculation. The majority of systems that go on to merge and potentially form a gamma-ray burst come from the population of closer binaries consisting of a compact object and a helium star.

The merger time distributions for the three different models are shown in Figure 4. Under all three assumptions about the strength of kicks, the merger times are predominantly long; that is, greater than 1 Myr. The distributions that we obtain are similar to distributions obtained by previous work in the field (e.g. figure 23 of Fryer et al. 1999).

### 3.2 Galactic trajectories

In order to predict the offsets of compact binary systems from their host galaxies at the time of final merger we integrate their motion in the gravitational potentials of their

<sup>1</sup> The Hubble time is taken to be 14 Gyr throughout.

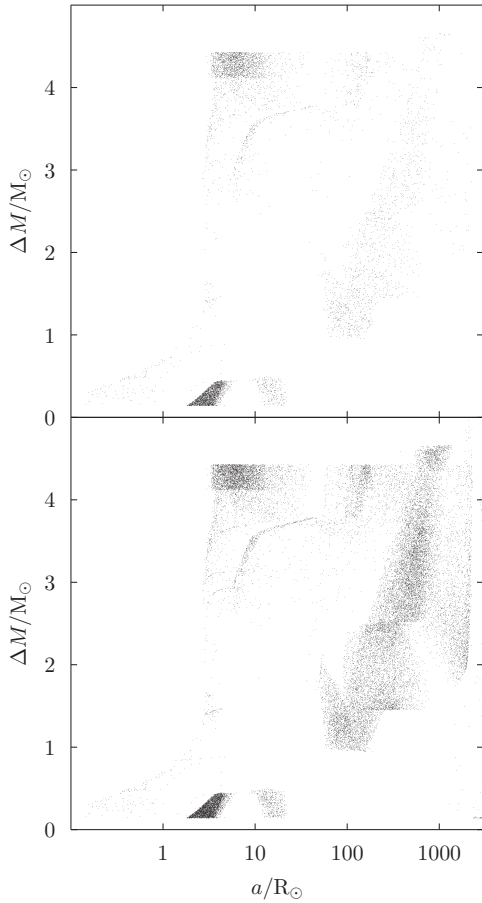


**Figure 3.** As in Figure 2 but for BH-NS progenitors. Dots show the mass lost in the final supernova  $\Delta M$  as a function of pre-supernova semi-major axis  $a$  for the binaries that potentially form a NS-NS binary. The bottom panel shows all binaries that are bound prior to the final supernova, the upper panel only the subset that remain bound subsequent to the final supernova. The ACC02 kick distribution was used for both kicks.

modelled host galaxies. For each host we produce a halo model as described in Section 2; the parameters of the models are listed in Table 2. We place the stars initially in an exponential disc and assign the initial location of each DCO binary with a probability proportional to the disc’s luminosity at that point, i.e. our DCO binaries originate tracing the light of their host galaxies as is seen for most supernovae (Fruchter et al. 2006; Kelly et al. 2008). Each DCO binary’s initial velocity is set equal to the sum of its circular velocity in the galactic potential and a kick velocity that originates in the effects of the supernovae on the binary’s centre-of-mass velocity; this is calculated during the population synthesis. The orientation of the orbital plane of the binary with respect to the disc of the host galaxy is taken to be isotropically distributed. The binary’s trajectory is then calculated and its position at the time of merger recorded. We view the galaxy from a direction chosen uniformly across a sphere and record the binary’s *projected* offset from the galaxy centre at this time. We compute  $10^5$  trajectories for each galactic model in order to obtain distributions of predicted burst off-

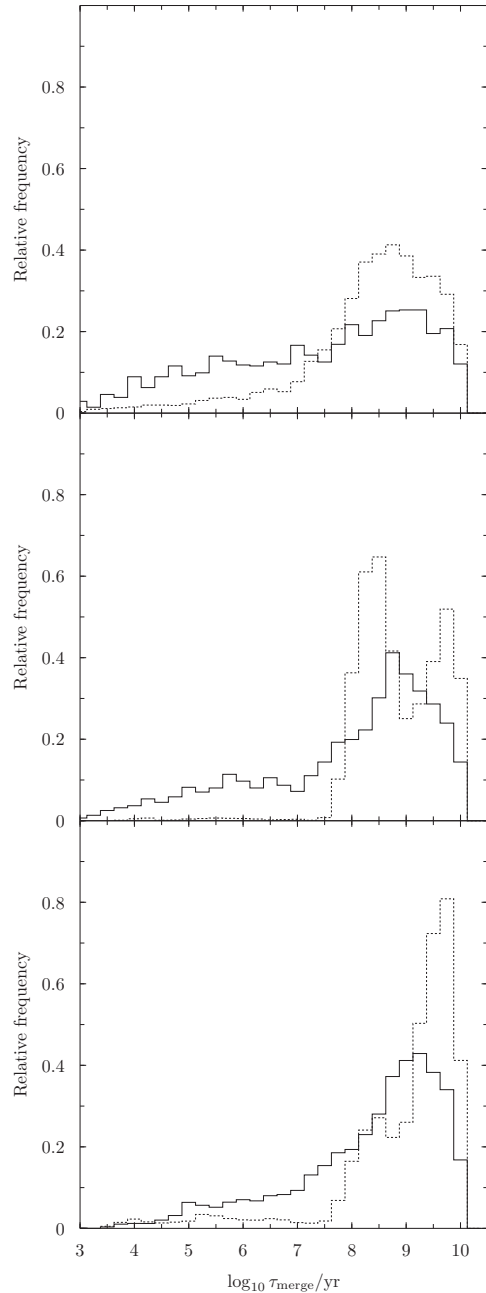


**Figure 4.** The distribution of merger times of the NS-NS and BH-NS binaries produced by our population synthesis calculations. Solid lines show NS-NS binaries, dotted lines BH-NS binaries. In the top panel the ACC02 kick distribution was used for both kicks, in the middle panel the ACC02 distribution was used for the first kick and the DPP05 distribution for the second kick, and in the bottom panel the DPP05 distribution was used for both kicks. Only binaries that merge within the Hubble time are included.

sets. These distributions are shown in Figures 5, 6 and 7, in addition to the offsets of observed bursts.

For some of the hosts the inclination of the host disc with respect to our galaxy is known. Hence we tested whether the viewing the host from a fixed angle as opposed

to a random angle affected our results. We found that the distribution of offsets did not change significantly.

## 4 DISCUSSION

The results of the simulations are presented in Figure 1, which shows the distribution of binaries in the  $a$  vs.  $e$  plane, and Figures 5 to 7, which contain the binary natal velocity distributions and predicted offset distributions.

### 4.1 Synthesised binary population

The distributions of compact object binaries in the  $a$ ,  $e$  plane that our population synthesis calculations generate are shown in Figure 1. A detailed discussion of whether the observed population is consistent with our prediction requires consideration of the biases in the detection of pulsars and is beyond the scope of this project, but it can be simply stated that it is necessary for all of the observed binaries to be able to form under the adopted description of binary evolution processes. The  $a$ ,  $e$  plots show that, for a kick distribution where the second kick is weak – that is, drawn from a DPP05-like population – it is not possible to make a NS–NS binary such as PSR B1913+16 (the Hulse–Taylor pulsar). This means that the binary in which it formed must have experienced a relatively strong second kick. It does not necessarily indicate that all NS natal kicks must be strong, as some intricacy of the evolution may cause some NSs to receive a strong natal kick and some a weak one, but for the purposes of this study it leads us to prefer a kick distribution where all the NSs receive a strong kick on formation. The  $a$ – $e$  distribution that we obtain using a strong kick is similar to that of, for example, Bloom et al. (1999), though with an additional population of long-period binaries. This difference is not significant for this project as the long-period population all have merger times greater than the Hubble time.

Examination of the binary birth velocity distributions presented in Figures 5 to 7, which are the result of the effects of both supernova mass loss and supernova natal kicks on the space velocity of the compact binaries, shows that there are significant differences between NS–NS and BH–NS binaries. In the cases where the second kick is weak (Figures 6 and 7) a significant population of the BH–NS binaries acquire velocities that are large relative to the NS natal kick velocities. These large velocities originate in the loss of a substantial quantity of mass during the formation of the NS when the binary is close and hence the stars’ velocities large. The lower compact companion mass in comparable systems that form NS–NS DCOs limits the amount of mass that can be lost without the binary breaking up and hence reduces the effect of this process. Therefore, for a small second kick the systems with the largest space velocities are BH–NS binaries. This is not the case, however, when the second kick is large (and hence more dominant over the effect of mass loss); there a much larger proportion of the highest-velocity systems are NS–NS binaries.

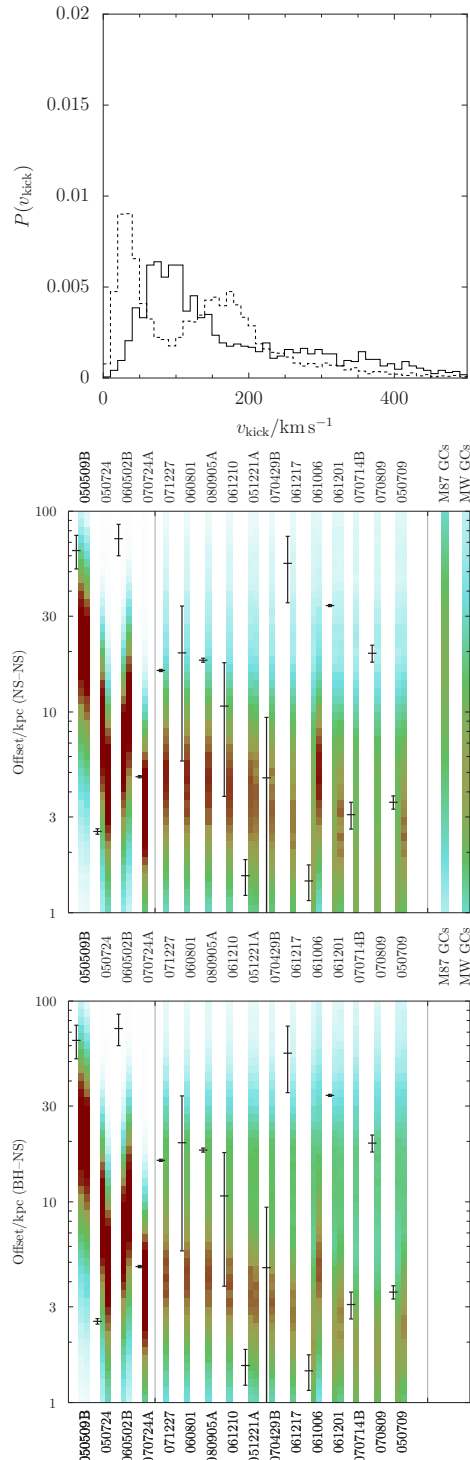


**Figure 5.** Top: the distributions of birth velocities for NS–NS (solid lines) and BH–NS (dashed lines) binaries. Both first and second natal kicks are taken from the ACC02 distribution. Middle: offset distributions of NS–NS binaries around different burst host galaxies compared to the observed burst offsets. The darkness of the colour is linearly related to  $dP(R)/d \log R$ . Error bars show one-sigma uncertainties in the observed offsets. Where both observed and predicted effective radii are available the additional right-hand stripe shows calculations made with the observed  $R_e$ . The two rightmost stripes represent the distribution predicted for the globular cluster systems of M87 and the Milky Way. Bottom: as middle but for BH–NS binaries.

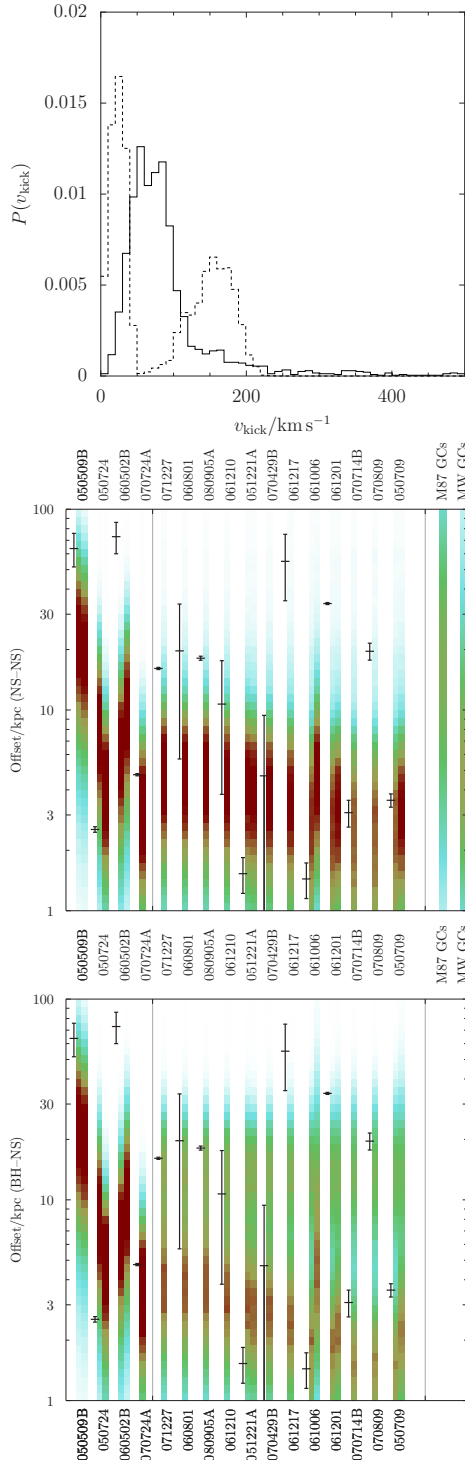


**Figure 6.** As in Figure 5, but the first kick is taken from the ACC02 distribution and the second from the DPP05 distribution.

#### 4.2 Predicted galactic offsets

The hosts in Figures 5 to 7 are sorted in order of decreasing blue-band magnitude. A generally large scatter can be seen in their observed offsets, though two of the three most luminous – and more massive – elliptical galaxies host short bursts at typically large offsets. These are also typically bursts with shorter durations, which have been suggested

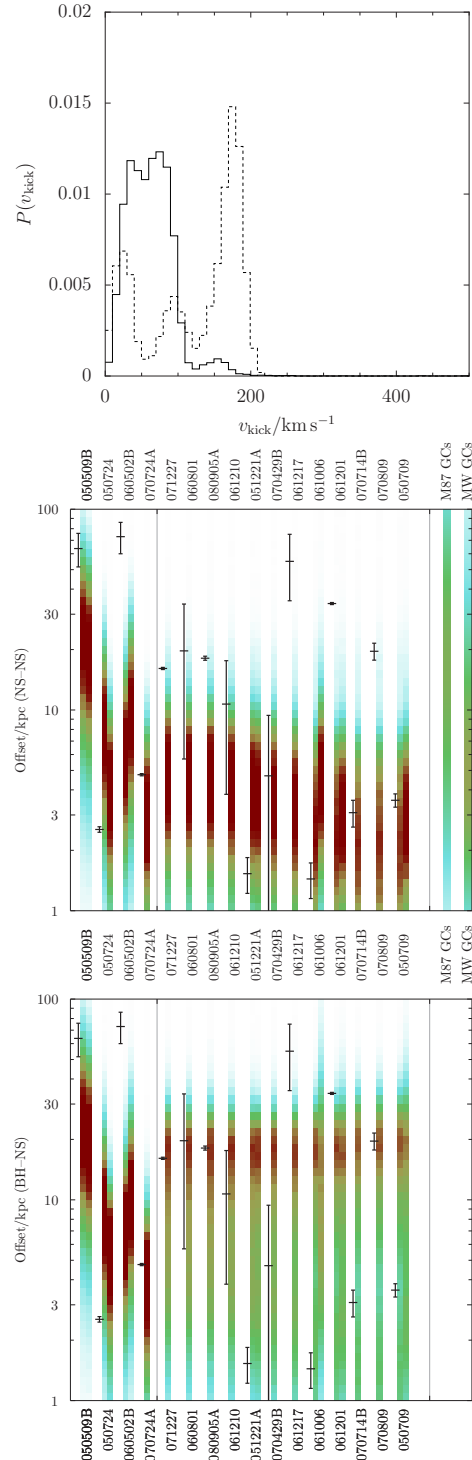


**Figure 7.** As in Figure 5, but with both kicks drawn from the DPP05 distribution.

to lie at larger radii from their hosts (Troja et al. 2008), where the short durations, and very faint X-ray afterglows would correspond to low ISM density about the progenitor. The large scatter observed is consistent with the models, as shown by the broad probability distributions.

There is a qualitative difference between the behaviour of binaries in the elliptical galaxies in our sample and those in spiral galaxies. The elliptical galaxies are much more

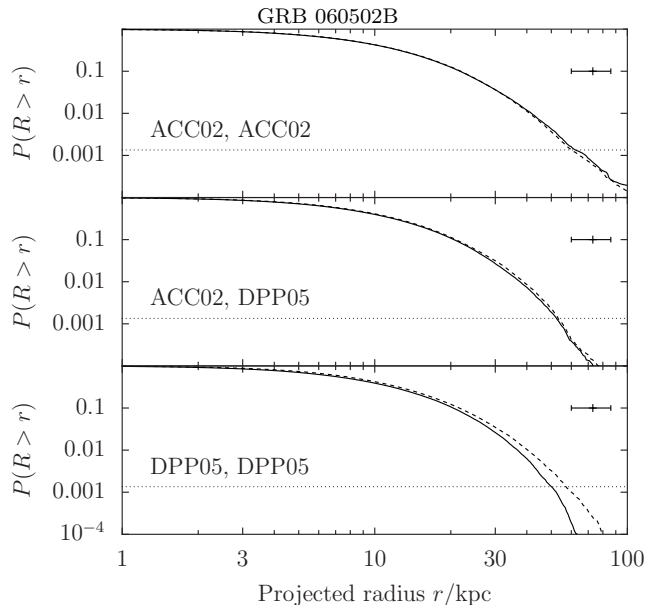


**Figure 8.** The probability of obtaining an offset larger than some projected radius  $r$  as a function of  $r$ , in our models of the host galaxy of GRB 060502B. Solid lines represent the distributions of NS–NS binaries, dashed lines those of BH–NS binaries. Distributions have been calculated using the observed  $R_e$ . The three panels show the three different pairs of kick distributions that we considered. The error bars, placed at arbitrary heights, show the one-sigma error on the observed offset. The dotted line marks the three-sigma probability.

massive and have halo circular velocities between 400 and 700  $\text{km s}^{-1}$ . These circular velocities exceed the vast majority of the binary natal velocities regardless of the kick distribution used. Hence the binaries’ galactic orbits are only mildly perturbed by the kicks and the offset distributions are determined largely by the effective radii of the hosts. The spiral galaxies, on the other hand, have much lower circular velocities of between 100 and 200  $\text{km s}^{-1}$ . Hence they have extended offset distributions given their small sizes, particularly for the BH–NS binaries and the stronger kick distribution.

Our models predict offset distributions that match all of the bursts observed around spiral galaxies, provided that either the natal kick is relatively strong, or the progenitors of the bursts with the largest offsets are BH–NS binaries rather than NS–NS binaries. The cumulative offset distributions for the spiral galaxies hosting the two bursts with the largest offsets are shown in Figures 9 (GRB 061217) and 10 (GRB 061201). However, the burst with the largest offset, GRB 060502B which has an elliptical host, is not well fitted by the models. The cumulative burst probability, calculated using the measured  $R_e$ , is shown in Figure 8. Fewer than 0.1% of possible hosts lie within its 1-sigma offset position, and fewer than 2% within its 3-sigma offset position. We cannot exclude the model at a 5-sigma level as the error box then overlaps a large fraction of the host galaxy.

Given the uncertainty in the distribution of natal kicks it is prudent to investigate the effects of a natal kick stronger than the ACC02 distribution. Following a suggestion from the referee, we re-calculated the cumulative offset distribu-

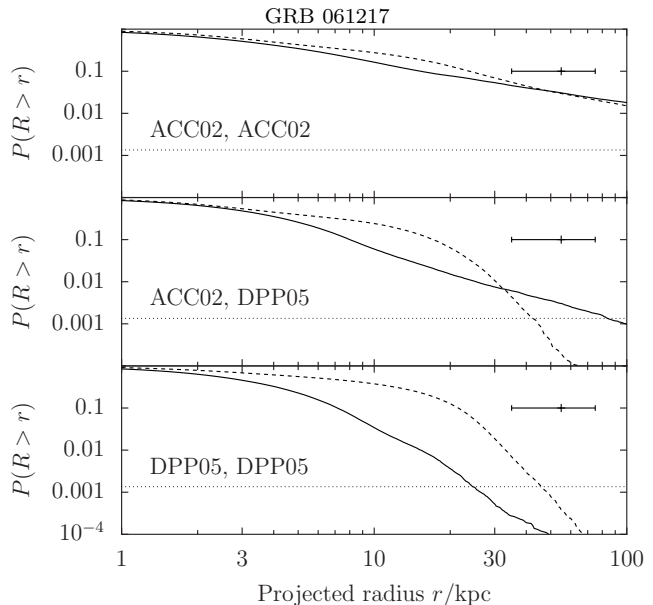


**Figure 9.** As Figure 8, but for GRB 061217. The calculations use a predicted  $R_e$  as no observation was available.

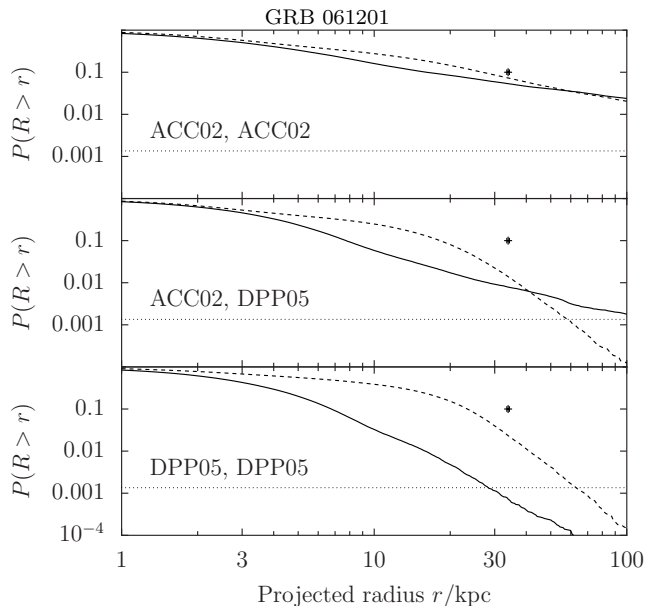


**Figure 10.** As Figure 8, but for GRB 061201.

tion using an ACC kick distribution scaled up by a factor of two – i.e. where the peak probability was at twice its normal value. The results are presented in Figure 11. The distribution of offsets from NS–NS mergers remains effectively unchanged as the stronger kicks merely serve to break up a larger fraction of the binaries. A small tail of BH–NS mergers at larger offsets is generated, but it is not significant enough to explain the burst.

Several other bursts also lie towards the edge of the predicted distribution. Only 8% of predicted burst locations lie outside the measured offset of GRB 061201, and only 16% outside the measured offset of GRB 070809 (although in

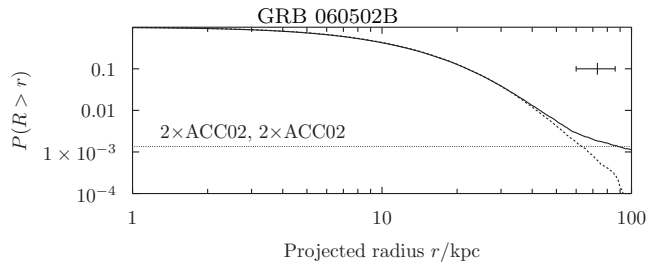


**Figure 11.** As Figure 8 but showing the effect of doubling the strength of the ACC02 kick distribution. The plot shows the probability of obtaining an offset larger than some projected radius  $r$  as a function of  $r$ , in our models of the host galaxy of GRB 060502B. Solid lines represent the distributions of NS–NS binaries, dashed lines those of BH–NS binaries. Distributions have been calculated using the observed  $R_e$ . The three panels show the three different pairs of kick distributions that we considered. The error bars, placed at arbitrary heights, show the one-sigma error on the observed offset. The dotted line marks the three-sigma probability.

that case the positional error bars are larger). Furthermore, there is some uncertainty over the properties of the host of GRB 050509B. Bloom et al. (2006) give its effective radius as 3.47 kpc, rather than the 20.98 kpc given by Fong et al. (2009). This, in combination with the velocity dispersion, which Bloom et al. (2006) measure to be  $250 \text{ km s}^{-1}$ , suggests that it may be more like the host of GRB 060502B than the model we have used. If so this would provide another large offset that would be hard to match with the DCO model. These points strengthen the case that there is an excess of large offsets compared to our predictions.

### 4.3 Selection effects and correlations

There are clearly possible selection effects in operation. For example, bursts expelled large distances from low mass galaxies may be essentially impossible to associate with their hosts with any confidence. This is the likely explanation for the apparently host-less GRBs 061201 and 080503 (Perley et al. 2009). A further selection effect worthy of inspection is the possibility that the majority of DCOs that form in elliptical galaxies have merged before we observe their hosts. If the DCOs that merge at small offsets come predominantly from the population with short merger times then we would not expect to see them in nearby, old giant ellipticals. To investigate this we have plotted the distribution of projected burst offsets for our model of the host of GRB 060502B as a function of time since a single star formation burst (Figure 12). The distributions for different times are essentially identical, as the galaxy rotation velocities are much larger than the supernova kick velocities. Furthermore, the fraction of SGRBs observationally associated with old, rather than young populations is at least  $\sim 25\%$ , based on the fraction of identified hosts that are elliptical galaxies. This strongly suggests that the rapidly merging population cannot dominate at the current epoch.

Other correlations of burst properties with those of their hosts have been reported elsewhere. In particular, Troja et al. (2008) suggest that bursts with extended emission typically form at smaller projected distances from their

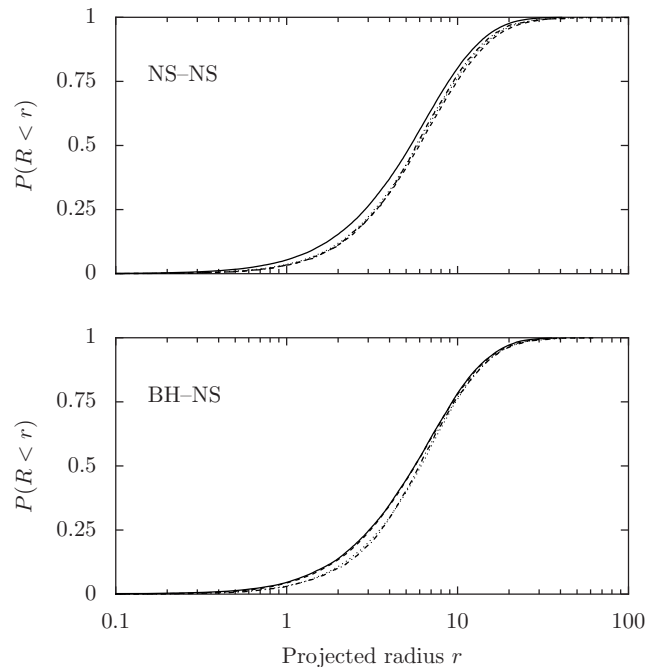


**Figure 12.** The cumulative probability distribution of projected burst offsets plotted for different times after a starburst. Solid lines represent bursts occurring within 100 Myr, dashed lines bursts occurring between 100 Myr and 1 Gyr after the starburst, dotted lines bursts occurring between 1 Gyr and 10 Gyr after the starburst and dash-dotted lines burst occurring more than 10 Gyr after the starburst. The upper panel shows the distributions for NS–NS progenitors, the lower panel those for BH–NS progenitors. The model used is that for the host of GRB 060502B.

hosts than very short bursts. They suggest that this may be due to the bursts with extended emission occurring via NS–BH mergers, which may travel less far. Our population synthesis indicates that this is not the case, and that BH–NS and NS–NS populations have broadly similar radial distributions, with the BH–NS population being *more* extended as explained in Section 4.1. For the preferred strong kick we find that the distributions are almost identical (see Figure 5).

A second reported correlation was that of Rhoads (2008), who showed that there is an anticorrelation between the absolute magnitude of the host, and the isotropic energy release of the burst. Our results confirm this, however, in the light of previous discussion it is possible to recast this correlation in terms of the observed offsets from host galaxies, notably, that the offset and energy appear to be anti-correlated as well. It is therefore interesting to investigate if the source of the correlation is the due physically to the difference in host absolute magnitude, the offset, or another physical mechanism which can explain both.

There is a correlation between the direction of the natal velocity of a DCO binary and the orientation of its orbital plane. In particular, if the natal kick is weak and hence the binary natal velocity is dominated by the loss of mass in the second supernova explosion, then the natal velocity should be perpendicular to the orbital axis. If the gamma-ray emission is beamed along the orbital axis then this correlation has the potential to increase the magnitude of the *observed*

offsets. This effect was considered at an early stage in these calculations and found to be small once realistic binary evolution and galactic trajectories were taken into account.

#### 4.4 Host galaxy selection

An ongoing problem with studies of SGRBs is the association of a given burst with its host. In a few cases optical afterglow positions provide high confidence associations showing that a burst lies on the stellar field of a given host. However, in many cases this was not possible, and different approaches have been taken. For example, in the case of GRB 060502B, Bloom et al. (2007) identify the host as the giant elliptical considered here with a large offset, whilst Berger et al. (2007) adopt a strategy of identifying the brightest extended object *within* the XRT error box, which leads to a different, fainter host at a smaller offset. This problem is most severe for GRBs 050509B and 060502B. The probability of random association with a background galaxy some distance from the burst position is frequently rather similar to the probability of a chance alignment within the error circle (Levan et al. 2007). In such circumstances it becomes very difficult to identify the host with high confidence, and it is likely that strong constraints will only come with the build up of a larger sample, in which it is possible to say if, for example, large elliptical galaxies are over-represented.

Of course, in part the difficulty in locating burst afterglows may be due to the progenitors of the bursts themselves. If NS-NS binaries are expelled from their hosts with large velocities then their optical afterglow brightness will be significantly suppressed due to the low ISM density, since the afterglows are caused by external shocks. In very low density media the cooling break may even move above the X-ray band, and result in very faint afterglows. Indeed, Troja et al. (2008) have suggested that bursts with shorter durations, and fainter X-ray afterglows lie systematically at larger distances from their hosts than the longer duration brighter bursts.

A recent and closely-related paper (Berger 2010) has discussed the possible origin of short GRBs with optical afterglows with significant offsets. They concentrate on bursts with optical afterglows as having smaller positional errors, and show that for all but one burst where the identity of the host is in doubt the lowest probabilities of chance coincidence is associated with bright galaxies at offsets of a few tens of kpc. Their results are in agreement with ours, in that they state that the observations fit a model where these offsets arise naturally in merging NS-NS binaries that have been kicked out of their host galaxies. They do not find any additional contribution at larger offsets necessary; on the other hand they do not carry out host-by-host modelling as we do and they neglect the bursts with only X-ray detections that have the largest offsets.

## 5 GLOBULAR CLUSTERS

An alternative explanation of the very large offsets of some SGRBs from their host galaxies is that they occur in compact binaries residing within the globular cluster systems of their host galaxies. Within the dense environments at the

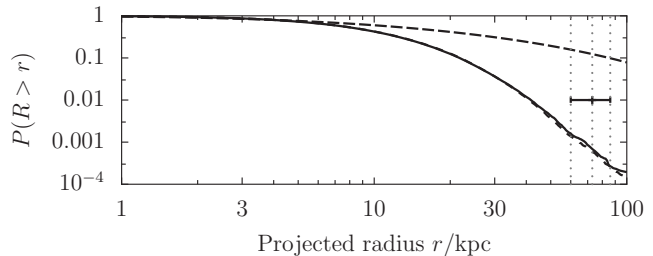


**Figure 13.** The long-dashed thick line shows the offset distribution of SGRBs, calculated under the assumption that they occur via the merger of dynamically-generated NS-NS binaries in the cores of globular clusters and hence follow their projected spatial distribution. The globular cluster population chosen is that of M87. The error bar, placed at arbitrary height, represents the offset of GRB 060502B from its putative massive elliptical host galaxy. The thin solid and short-dashed lines are the results from the standard model of a field population of DCO binaries as presented in Figure 8. The thin solid line shows NS-NS binaries and the thin dashed line BH-NS binaries.

cores of globular clusters NS-NS binaries can form through dynamical interactions (Davies 1995). Such a scenario for the formation of SGRBs was proposed by Grindlay et al. (2006), who show that, based on some simple assumptions about the formation channels of NS-NS binaries within GCs and plausible number densities of neutron stars and low-mass X-ray binaries, a significant fraction of SGRBs could form via this channel.

### 5.1 Radial distribution

To assess the viability of this alternative, we have plotted the galactic distribution of gamma-ray bursts assuming that they follow the globular cluster population of two galaxies; M87 and the Milky Way. M87 is a giant elliptical galaxy in the Virgo cluster, with a population of roughly 14000 globular clusters (Harris 2009). The distribution of its clusters has a very large spatial extent, extending to at least 100 kpc. The Milky Way has a more modest distribution of about 160 clusters with the most distant also being at roughly 100 kpc (Djorgovski & Meylan 1994). We plot the projected radial distributions of the two globular cluster systems in Figures 5 to 7. For M87 we utilise the fits given by Harris (2009), whereas for the Milky Way we take the fit to the 3-dimensional number density distribution provided by Djorgovski & Meylan (1994) and project it. For simplicity we assume that the dynamical formation of the NS-NS binaries which may lead to SGRBs proceeds in a similar manner across all the GCs. Hence we obtain projected offset distributions, which are plotted on the right-hand side of Figures 5 to 7, along with the cumulative probability distribution in Figure 13. Both distributions are much more extended than the kick-derived offset distributions, and are consistent with the most-offset bursts.

### 5.2 Formation rates

To assess the viability of globular cluster systems as formation sites for SGRB progenitors it is instructive to estimate the formation rates within the clusters and galaxies.

To simulate the populations here we evolved  $4 \times 10^7$  binaries, which when using strong (ACC02) kicks produced 1659 NS–NS binaries and 4253 BH–NS binaries, counting only those binaries that merge within  $1.4 \times 10^{10}$  years. Once we have corrected for the fact that we only sample the heavy end of the IMF this leads to specific merger rates of  $15 f_b$  and  $38 f_b (10^9 M_\odot)^{-1} t_{\text{Hubble}}^{-1}$ . Here  $f_b$  is the fraction of stellar mass in binary systems. For globular clusters we extrapolate from the observation of a single dynamically-formed NS–NS binary in a Galactic globular cluster, M15-C, with a merger time of roughly 300 Myr, amongst the roughly 150 Galactic globular clusters. Utilising the observations of Rhode et al. (2005) which suggest that the number of globular clusters per  $10^9 M_\odot$  of stellar mass,  $T$ , lies between 1 (for field spiral galaxies) and 4 (for cluster elliptical galaxies) gives a NS–NS merger rate from globular clusters of  $0.31T (10^9 M_\odot)^{-1} t_{\text{Hubble}}^{-1}$ . This is obviously much smaller than the field merger rate even for elliptical galaxies but there is a severe underestimate for several reasons. Pulsar surveys of galactic globular clusters are incomplete, and the inclusion of only a single system in our calculations samples only a small range of possible merger times. Based on simple scattering simulations of binaries in globular clusters Grindlay et al. (2006) show that this simple extrapolation is an underestimate by a factor of between 10 and 100, which brings the rate estimate to a similar magnitude to that from field binaries. Furthermore, the massive elliptical galaxy M87 has a value of  $T \simeq 8$  for the blue globular cluster sequence alone (Brodie & Strader 2006). Clearly more detailed simulations of globular clusters are required to form a more accurate estimate of their production rates of NS–NS binaries, but this crude analysis shows that the rates could be comparable, and that given a sample of nearly 20 SGRBs it would not be surprising for the progenitor binary of one or more of them to have formed in a globular cluster. Furthermore, the burst that we suggest is most likely to have formed in a globular cluster, GRB 060502B, has a giant elliptical host which would be expected to have a larger specific globular cluster fraction.

## 6 SUMMARY

We have synthesised populations of NS–NS and BH–NS binaries and used them to predict the galactic offset distributions of short gamma-ray bursts, given the observed properties of their host galaxies. The offsets of all but one short gamma-ray burst are found to be consistent with this picture. However, the burst GRB 060502B apparently has an inconsistently large offset. It is plausible that this inconsistency results from a mis-identification of the host galaxy, but we show that the large offset is consistent with the merger of a NS–NS binary that has been created by dynamical encounters within a globular cluster. The offset distribution arising from the globular cluster systems of the Milky Way and a local massive elliptical galaxy, M87, are consistent with the observed offsets of all short GRBs, including GRB 060502B, and that the production rate of such binaries may be comparable with that of field DCO binaries.

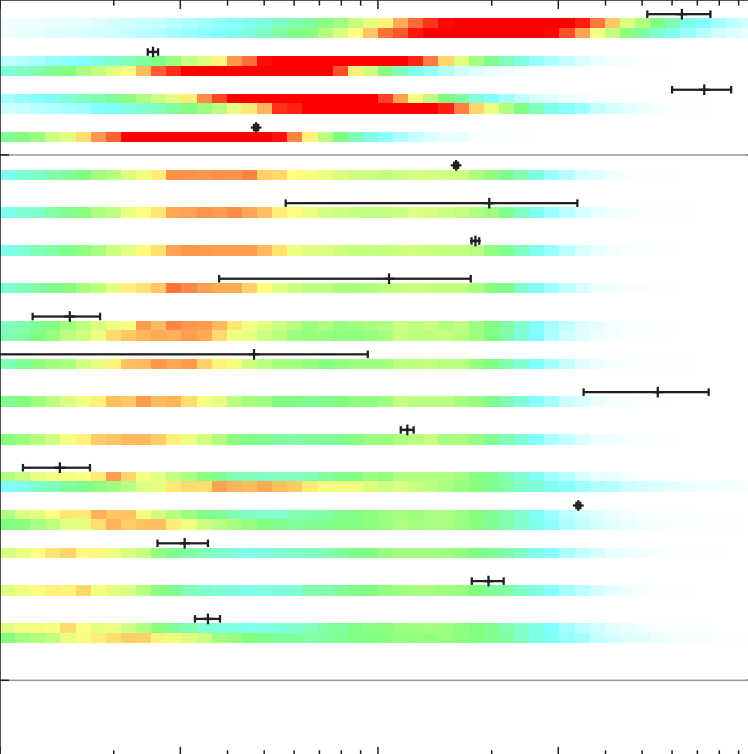
## ACKNOWLEDGEMENTS

The authors would like to thank the anonymous referee for their constructive comments, which helped to improve this paper. RPC thanks the Wenner-Gren Foundation for support. This work was supported by the Swedish Research Council (grant 2008-4089). The calculations presented in this paper were carried out using computer hardware purchased with grants from the Royal Physiographic Society of Lund.

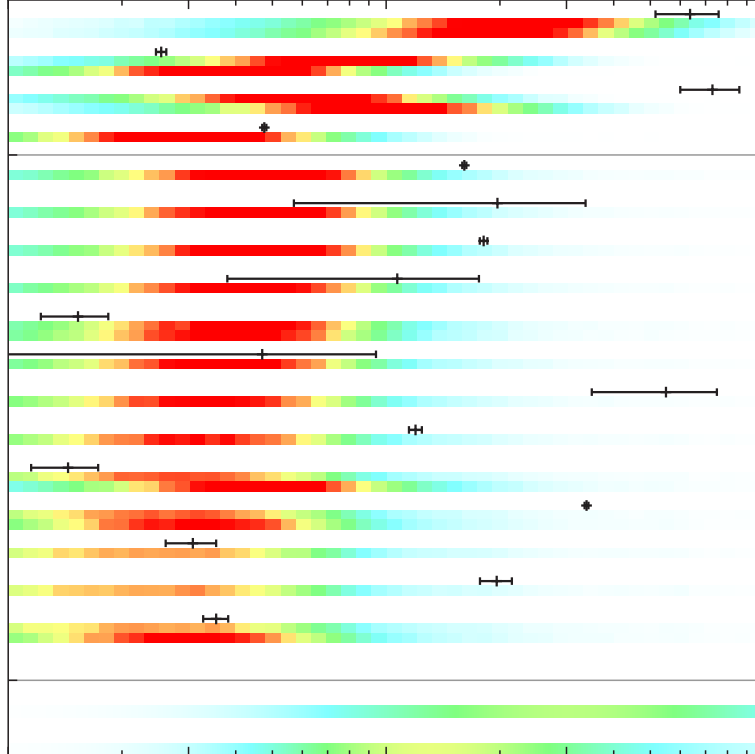
## REFERENCES

- Arzoumanian, Z., Chernoff, D. F., Cordes, J. M., 2002, *ApJ*, 568, 289
- Barthelmy, S. D., et al., 2005, *Nature*, 438, 994
- Belczynski, K., Kalogera, V., Bulik, T., 2002, *ApJ*, 572, 407
- Belczynski, K., Perna, R., Bulik, T., Kalogera, V., Ivanova, N., Lamb, D. Q., 2006, *ApJ*, 648, 1110
- Belczynski, K., Kalogera, V., Rasio, F. A., Taam, R. E., Zezas, A., Bulik, T., Maccarone, T. J., Ivanova, N., 2008, *ApJS*, 174, 223
- Berger, E., 2010, *ArXiv e-prints*
- Berger, E., Cenko, S. B., Fox, D. B., Cucchiara, A., 2009, *ApJ*, 704, 877
- Berger, E., et al., 2005, *Nature*, 438, 988
- Berger, E., et al., 2007, *ApJ*, 664, 1000
- Bloom, J. S., Sigurdsson, S., Pols, O. R., 1999, *MNRAS*, 305, 763
- Bloom, J. S., et al., 2006, *ApJ*, 638, 354
- Bloom, J. S., et al., 2007, *ApJ*, 654, 878
- Brodie, J. P., Strader, J., 2006, *ARA&A*, 44, 193
- Cenko, S. B., et al., 2008, *ArXiv e-prints (astro-ph/0802.0874)*
- D’Avanzo, P., et al., 2009, in G. Giobbi, A. Tornambe, G. Raimondo, M. Limongi, L. A. Antonelli, N. Menci, & E. Brocato, ed., *American Institute of Physics Conference Series*, vol. 1111 of *American Institute of Physics Conference Series*, p. 524
- Davies, M. B., 1995, *MNRAS*, 276, 887
- Dewi, J. D. M., Podsiadlowski, P., Pols, O. R., 2005, *MNRAS*, 363, L71
- Djorgovski, S., Meylan, G., 1994, *AJ*, 108, 1292
- Fong, W., Berger, E., Fox, D. B., 2009, *ArXiv e-prints (astro-ph/0909.1804)*
- Fox, D. B., et al., 2005, *Nature*, 437, 845
- Frychter, A. S., et al., 2006, *Nature*, 441, 463
- Fryer, C. L., Woosley, S. E., Hartmann, D. H., 1999, *ApJ*, 526, 152
- Gehrels, N., et al., 2005, *Nature*, 437, 851
- Gerhard, O., Kronawitter, A., Saglia, R. P., Bender, R., 2001, *AJ*, 121, 1936
- Graham, J. F., et al., 2009, *ApJ*, 698, 1620
- Grindlay, J., Portegies Zwart, S., McMillan, S., 2006, *Nature Physics*, 2, 116
- Hansen, B. M. S., Phinney, E. S., 1997, *MNRAS*, 291, 569
- Harris, W. E., 2009, *ApJ*, 703, 939
- Hurley, J. R., Tout, C. A., Pols, O. R., 2002, *MNRAS*, 329, 897
- Kelly, P. L., Kirshner, R. P., Pahre, M., 2008, *ApJ*, 687, 1201

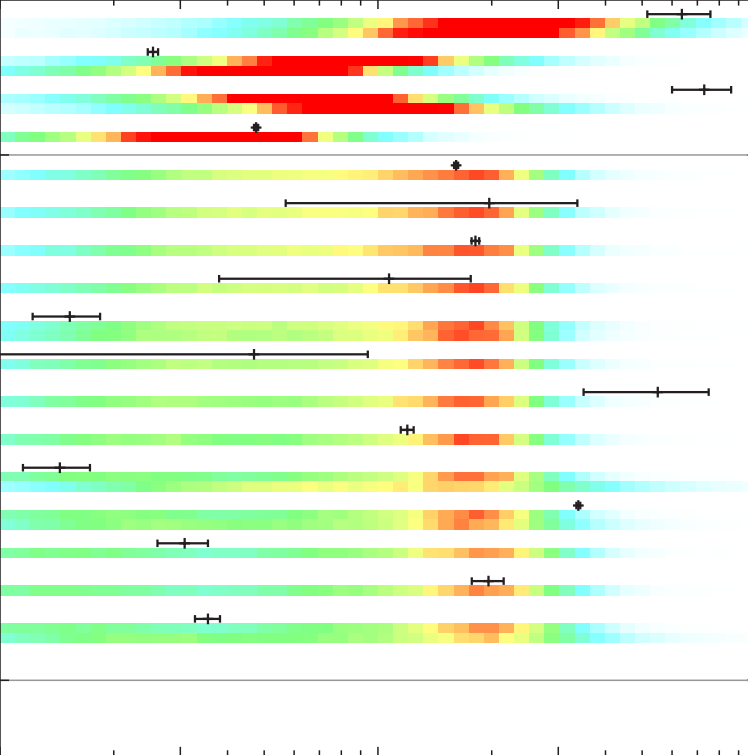
- Kormendy, J., Freeman, K. C., 2004, in S. Ryder, D. Pisano, M. Walker, & K. Freeman, ed., *Dark Matter in Galaxies*, vol. 220 of *IAU Symposium*, p. 377
- Kroupa, P., Tout, C. A., Gilmore, G., 1993, *MNRAS*, 262, 545
- Levan, A. J., et al., 2007, *MNRAS*, 378, 1439
- Mirabel, I. F., Rodrigues, I., 2003, *Science*, 300, 1119
- Perley, D. A., et al., 2009, *ApJ*, 696, 1871
- Rhoads, J. E., 2008, ArXiv e-prints (astro-ph/0807.2642)
- Rhode, K. L., Zepf, S. E., Santos, M. R., 2005, *ApJ*, 630, L21
- Soderberg, A. M., et al., 2006, *ApJ*, 650, 261
- Thomas, J., Saglia, R. P., Bender, R., Thomas, D., Gebhardt, K., Magorrian, J., Corsini, E. M., Wegner, G., 2009, *ApJ*, 691, 770
- Troja, E., King, A. R., O'Brien, P. T., Lyons, N., Cusumano, G., 2008, *MNRAS*, 385, L10
- Villasenor, J. S., et al., 2005, *Nature*, 437, 855
- Zheng, Z., Ramirez-Ruiz, E., 2007, *ApJ*, 665, 1220



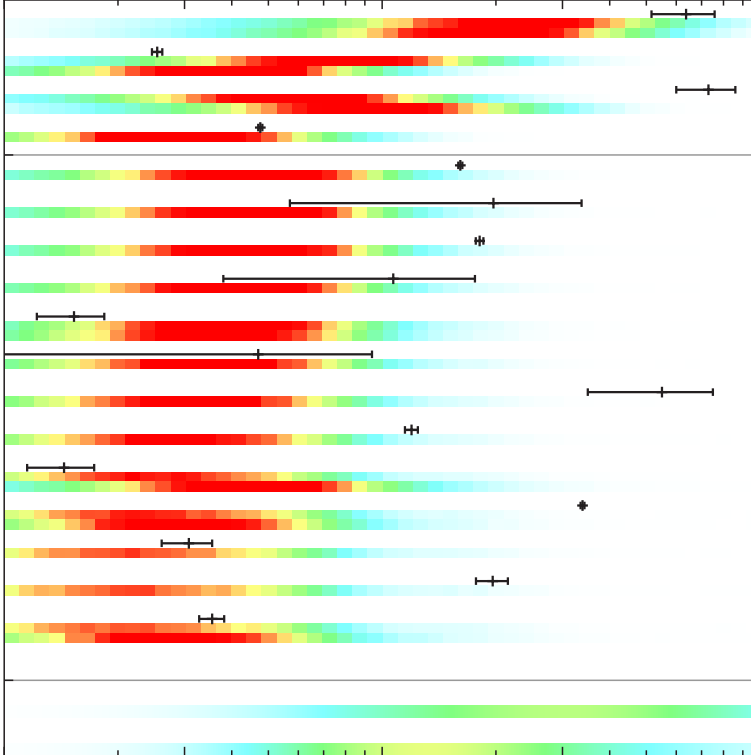
050509B  
 050724  
 060502B  
 070724A  
 071227  
 060801  
 080905A  
 061210  
 051221A  
 070429B  
 061217  
 090510  
 061006  
 061201  
 070714B  
 070809  
 050709  
 M87 GCs  
 MW GCs



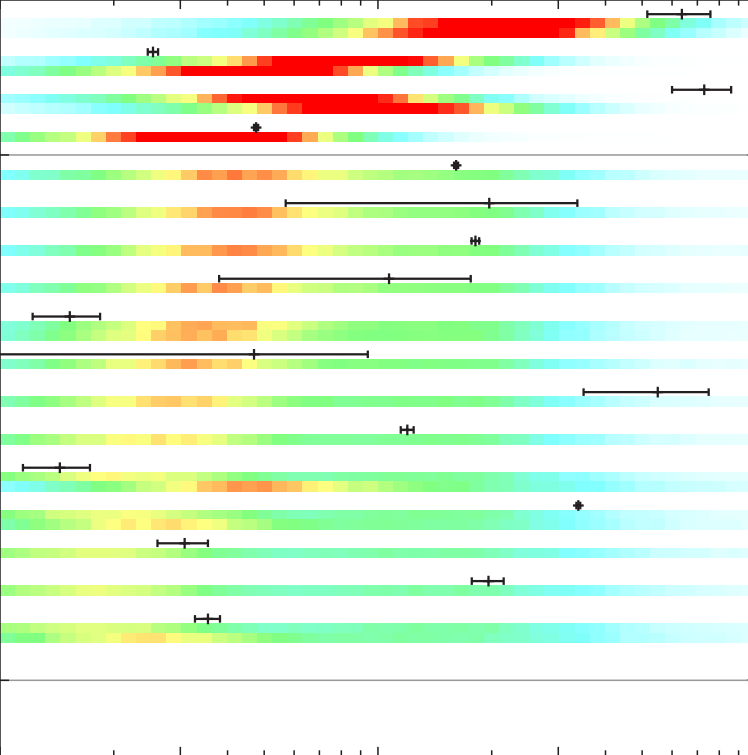
050509B  
 050724  
 060502B  
 070724A  
 071227  
 060801  
 080905A  
 061210  
 051221A  
 070429B  
 061217  
 090510  
 061006  
 061201  
 070714B  
 070809  
 050709  
 M87 GCs  
 MW GCs



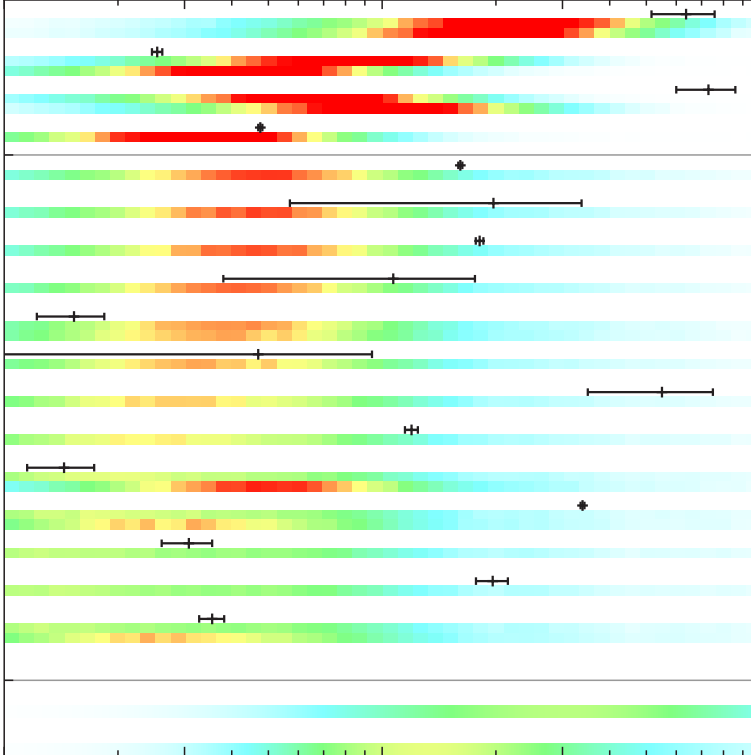
050509B  
 050724  
 060502B  
 070724A  
 071227  
 060801  
 080905A  
 061210  
 051221A  
 070429B  
 061217  
 090510  
 061006  
 061201  
 070714B  
 070809  
 050709  
 M87 GCs  
 MW GCs



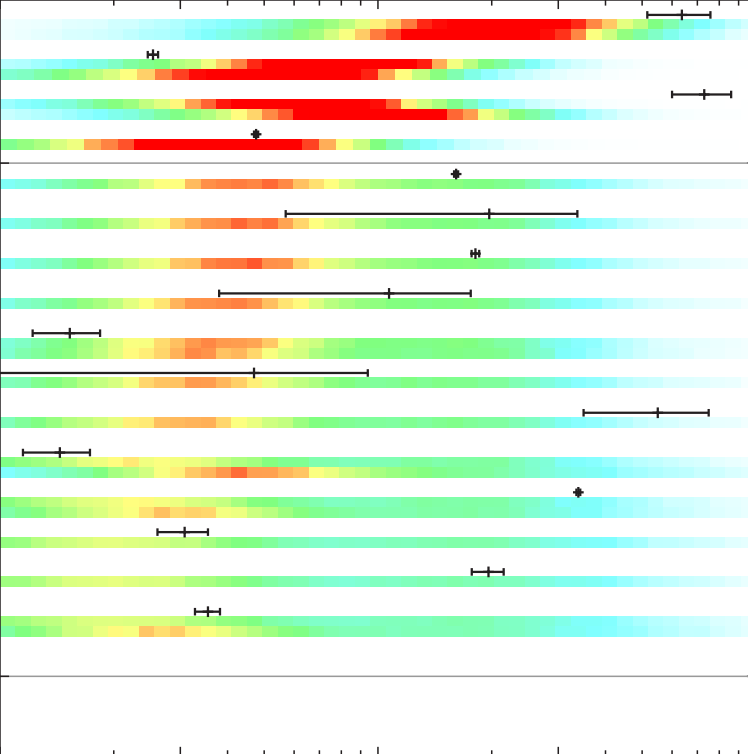
050509B  
 050724  
 060502B  
 070724A  
 071227  
 060801  
 080905A  
 061210  
 051221A  
 070429B  
 061217  
 090510  
 061006  
 061201  
 070714B  
 070809  
 050709  
 M87 GCs  
 MW GCs



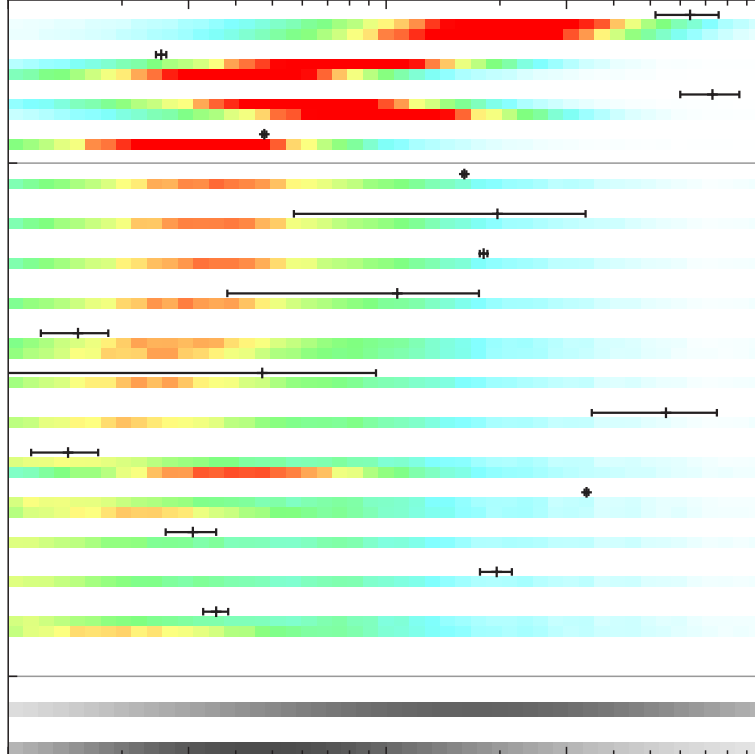
050509B  
 050724  
 060502B  
 070724A  
 071227  
 060801  
 080905A  
 061210  
 051221A  
 070429B  
 061217  
 090510  
 061006  
 061201  
 070714B  
 070809  
 050709  
 M87 GCs  
 MW GCs



050509B  
 050724  
 060502B  
 070724A  
 071227  
 060801  
 080905A  
 061210  
 051221A  
 070429B  
 061217  
 090510  
 061006  
 061201  
 070714B  
 070809  
 050709  
 M87 GCs  
 MW GCs



050509B  
050724  
060502B  
070724A  
071227  
060801  
080905A  
061210  
051221A  
070429B  
061217  
061006  
061201  
070714B  
070809  
050709  
M87 GCs  
MW GCs



050509B  
050724  
060502B  
070724A  
071227  
060801  
080905A  
061210  
051221A  
070429B  
061217  
061006  
061201  
070714B  
070809  
050709  
M87 GCs  
MW GCs